Article

Non Linear Strain Measures on Concrete Structures by Means of Embedded Optical Fiber Sensors

Vincenzo Minutolo [1,*], Renato Zona [1]

[1] Department of Engineering, University of Campania, "Luigi Vanvitelli" , via Roma, 81031 Aversa, Italy
* Correspondence: vincenzo.minutolo@unicampania.it;

Abstract: Optical fiber sensors have become a widely-used tool to perform life-long monitoring of large structures. Different set-ups of sensors can be used to obtain information at different scopes. In this paper, the application of a portable Brillouin optical time domain analysis sensor applied to reinforced concrete beams is presented. The sensor is made up of a single-mode optical fiber applied to the structure that enables the measurement of tensile and compressive axial strain along the beams. The fiber is embedded into a concrete casting and fixed along the reinforcement bars so that a complete correlation can be obtained regarding strain and displacements in linear and non-linear flexural response. The use of four sensing fibers positioned along the beam's length at different vertical positions makes it possible to read the strain variation within the cross-section. In accordance with Bernoulli's hypothesis, this allows curvature diagrams to be obtained across the structure. The measured curvature is used to set up the moment–curvature relationship, which highlights the possibility of the sensor monitoring structures continuously in space and time.

Keywords: Concrete structures**,** structure monitoring, optical fiber sensors, distributed sensors, Brillouin scattering.

1. Introduction

The basis of structural health monitoring (SHM) has been laid by Housner et al. [1], where it is defined as the continuous measurement and analysis of the main structural and environmental parameters under operating conditions in order to detect anomalous behaviour in the initial phases and then as a prevention tool.

The structural health monitoring of materials is therefore necessary during the design phase, during construction and especially as an integral part of preventive maintenance procedures in service and in the assessment of damages.

The methods for SHM in materials include ultrasonic testing [2,6], thermography [7,9] and measurements of static deformation and dynamic vibrations [10,13]. Static stresses and dynamic vibration analysis are often limited to the reading of point sensors, such as strain gauges, accelerometers or contactless laser Doppler vibrometers [14,15].

Distributed strain measurements using optical fiber sensors, based on Brillouin optical time domain analysis (BOTDA), has great advantages with respect to traditional gauges such as resistive strain gauges or mechanical ones. The optical fiber plays the role of a sensor and also of the communication medium and is very cheap since the sensor is made of nothing but data transmission fiber. The feasibility of this kind of sensor is particularly suitable to concrete and other structures in Civil Engineering; the construction process, indeed, consists of several phases in a very unclean environment and is subjected to severe shocks and manipulation that can damage the sensor. In many papers, a detailed review of optical fiber sensors is presented where the properties of Brillouin optical time domain analysis (BOTDA) sensors are described; it can be seen that the use of a distributed sensor has great advantages with respect to the installation economy, set-up design and realization and data acquisition. Several experiments, as described in [16,17], show that building activity often

 doi:10.20944/preprints201807.0331.v1

damages electrical strain gauges or vibrating wire deformometers. In practice, structures are investigated experimentally only at the completion of construction, during final testing, when gauges are applied for a short elapsing time, whereas the life-long monitoring of the finished structure is not as frequently performed as it should be. As a matter of fact, life-long measurement is the new challenge in Civil Engineering, especially with respect to construction maintenance and management. It is clear that life-long monitoring requires that the sensors are positioned in situ and left in place for a long time; consequently, they need to be protected from the injuries caused by time and their environment [18].

Optical fibers for telecommunications, which are the sensing devices when BODTA is used, are very robust and do not suffer time degradation, but the fiber is rather fragile and requires some protection against mechanical shocks. For the scope, it is desirable that the fiber is protected by means of coating or by embedding the fiber itself into the concrete cast. An experimental arrangement that places embedded fibers into concrete structures is presented in several works where the feasibility of such a set-up is shown [19,23].

Barrias and Bao [24,25] describe the evolution of the SHM with a review of the major experiments and results carried out to date to demonstrate the effectiveness of the use of optical fiber sensors.

Several experiments have been performed in the BOTDA field with embedded sensors for different types of structures: reinforced concrete wall [26], prestressed concrete bridge [27], integrated optical fiber in functionalized carbon structures (FCS) [28] and also for the detection of vibration, surface cracking and buckling phenomena [29,31] in reinforced concrete, pre-stressed concrete (PSC) [32] and post-tensioned PSC [33].

In the present work, laboratory experiments are presented that concern reinforced concrete beams under flexural solicitation; the structures have been instrumented by embedded optical fibers, and the experimental configuration has been set up in order to account for the Bernoulli beam theory. It is shown that the embedded fiber sensor is able to reconstruct beam cross-section deformation; hence, curvature mapping is obtained along the whole beam with very little effort and a cheap cost.

In the following, a number of experimental measurements are reported. The experiments concern a set of four laboratory beams made of reinforced concrete. The beams have been loaded by two point forces, placed to obtain a large zone where pure bending alone acts as internal solicitation. Consequently, the beams have presented a pure bending failure, with a small influence of the shear on the collapse, as shown by the crack patterns recorded at the end of each test.

The experimental results show that the sensor is able to follow the load path from a low load level until plastic collapse. For this target, the beams have been instrumented by using four optical fibers at different heights along the structure. The curvature of the deformed shape of the beams is calculated by the variability of longitudinal strain along the height, in accordance with Bernoulli theory. As was expected, the actual deformation of the beam's cross-section remains almost planar, even at the non-linear stage of the stress. This result confirms the possibility of this kind of sensor being able to monitor large deformation.

2. Materials and Methods

Laboratory experiments have concerned reinforced concrete (RC) beams, casted by using designed concrete in order to obtain the prescribed of resistance $f_{ck} = 25MPa$. Figure 1 shows the casting phase, the reinforcement pattern and the fiber positioning.

Preprints (www.preprints.org) | NOT PEER-REVIEWED | Posted: 18 July 2018 doi:10.20944/preprints201807.0331.v1

Figure 1. Building of the specimen: (a) description of the reinforcement pattern; (b) casting phase and optical fiber embedding.

The beam shape is summarized hereafter:
Length $l = 1.82m$, square cross section, side $0.20m$. The reinforcement consists of four longitudinal steel bars, at the vertex of the beam; the bars have diameter $\phi_l = 12mm$. Finally, eight steel brackets whose diameter is $\phi_b = 8mm$ complete the reinforcement. The sensing device has been designed to monitor the axial strain within the beam at different locations along the longitudinal directions at different vertical positions. Then, it has been possible to get the longitudinal curvature of the beam axis provided by Bernoulli's hypothesis to hold; for the scope, each beam has been instrumented by coiling a single optical fiber four times along the whole beam's length. The sensor disposition allowed us to record four strain patterns at different heights. The fiber has been glued to the brackets and along the longitudinal bars by epoxy resin; moreover, a grid made of iron wires has been applied through the brackets so that the optical fiber could be suspended at the prescribed position, as depicted in Figure 2.

Figure 2. Fiber fixing: (a) the upper fiber is glued to the reinforcement; (b) an iron wire grid to fix the lower fibers.

The transversal position of the fibers is represented in Figure 4, where the structural scheme of the specimen is drawn as well.
The fiber position along the section height, measured from the bottom of the beam, is shown in the following Table 1.

Preprints (www.preprints.org) | NOT PEER-REVIEWED | Posted: 18 July 2018 doi:10.20944/preprints201807.0331.v1

Figure 3. Testing apparatus, load frame and hydraulic jacks

The loading equipment consists of a steel frame, where rolling cylindrical supports are positioned at the testing span distance, in order to provide the supports that allow horizontal displacements. Hence, the beam is subjected only to transversal actions (i.e. zero axial force).

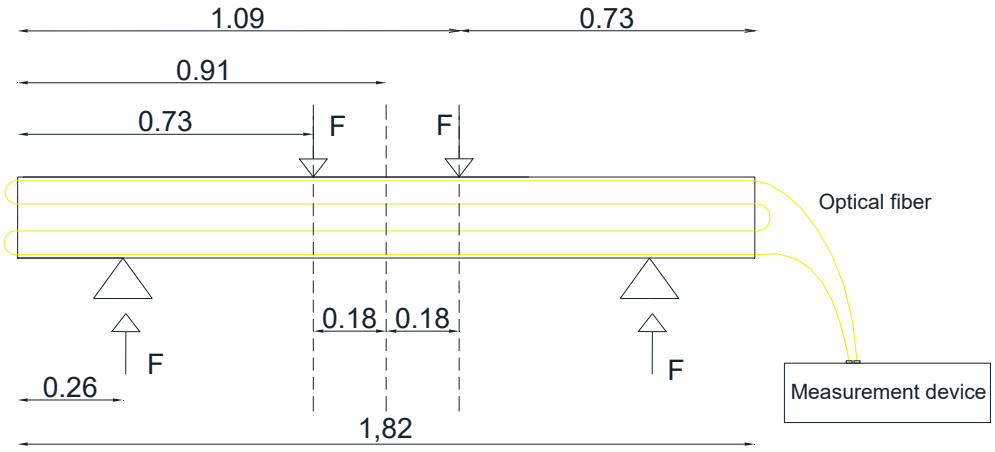

Figure 4. Testing scheme with fiber positions.

The load has been applied by means of two hydraulic jacks whose position is depicted in Figure 4. The experiment has been designed so that, at the middle of the beam span, constant bending moment results; such a loading pattern allows us to decouple the bending failure mechanism from shear effects.

Table 1. Position of the fiber sensors measured from the bottom.

Fiber n.	Distance from bottom mm
1	160
2	126
3	74
4	20

In order to have a redundant control of the electronic measures, the structure has been equipped with a displacement dial gauge, positioned at the middle span of the beam, as represented in Figure 5.

Preprints (www.preprints.org) | NOT PEER-REVIEWED | Posted: 18 July 2018 doi:10.20944/preprints201807.0331.v1

Figure 5. Dial displacement gauge position.

During the experiment, a time variable load has been applied through the servo-controlled jacks. The load has been programmed in order to apply increasing load during a prescribed set of loading–unloading steps. The load time history is represented in the diagram in Figure 6.

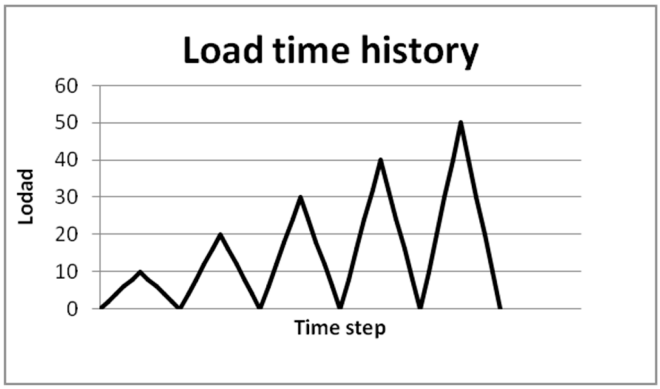

Figure 6. Load time history.

The structure has been tested with respect to bending, where the loads have been applied so that the bending moment was the main internal stress. Under such hypotheses, the main strain of the structure is the longitudinal one, ε ; under these conditions, the optical fibers give better results. The analytical solution of the collapse of the beam is obtained according to the reinforced concrete homogenization theory and to the prescription of Eurocode 2 (EC2).

3. Results

The constitutive mechanical parameter of the concrete is yield stress:

$$\sigma_y = 13.75MPa \tag{1}$$

The stress–strain curve is, on the compression side,

$$\begin{aligned} \sigma_c &= \sigma_{cy} && ,-0.0035 < \varepsilon < -0.002 \\ \sigma_c &= \left(1000\sigma_y\right)\varepsilon + \left(250000\sigma_y\right)\varepsilon^2 && ,-0.002 < \varepsilon < 0 \end{aligned} \tag{2}$$

and vanishes identically on the tension side.

The steel of the bars is supposed to be an elastic, perfectly plastic material with a Young's modulus E_s=210 GPa and stress yielding at

Preprints (www.preprints.org) | NOT PEER-REVIEWED | Posted: 18 July 2018 doi:10.20944/preprints201807.0331.v1

$$\sigma_{sy} = 380MPa \tag{3}$$

The stress–strain curve for the steel is altered by the following inequalities:

$$\begin{aligned} \sigma_s &= -\sigma_{sy} \quad ,-0.01 < \varepsilon < -0.002 \\ \sigma_s &= E_s \varepsilon \quad ,-0.002 < \varepsilon < 0.002 \\ \sigma_s &= \sigma_{sy} \quad ,0.002 < \varepsilon < 0.01 \end{aligned} \tag{3}$$

The stress strain curves for the two materials are drawn in figure 7.

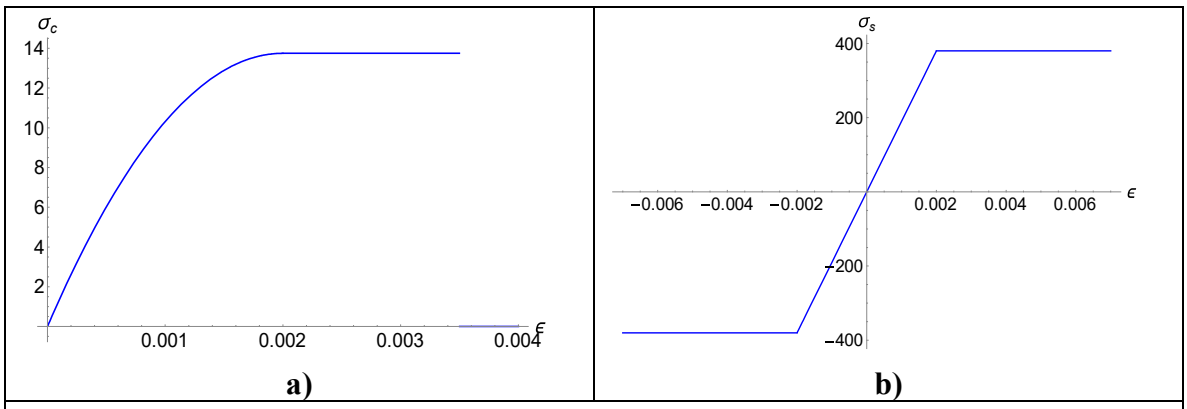

Figure 7: stress strain curves of the materials, a) concrete, b) steel

By means of the above definitions and by integrating the stress moment about the x axes along the beam thickness, one can calculate the moment–curvature relationship. The moment–curvature diagram is drawn in Figure 8.

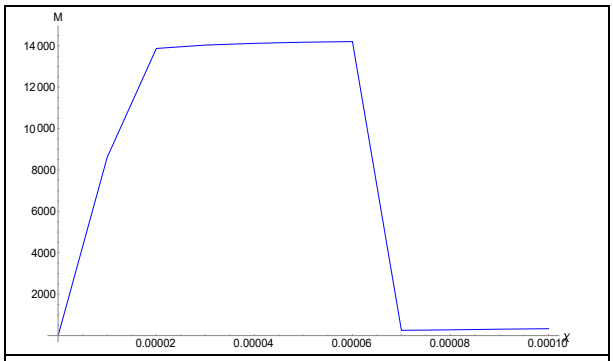

Figure 8: Bending moment versus curvature diagram

The maximum moment calculated using equations (2) and (3) is

$$M_m = 14.20kNm \tag{4}$$

An analogous calculation, made by means of standard formulas in European code EC2, gives the following results (see Table 2) that are in a good accordance with those reported above.

Preprints (www.preprints.org) | NOT PEER-REVIEWED | Posted: 18 July 2018 doi:10.20944/preprints201807.0331.v1

Table 2: Mechanical properties of the RC beam cross section by EC2.

Item	Value
Limit moment	13.9 kNm
Limit neutral axes y_n^p	0.168 m
Elastic neutral axes y_n^e	0.14 m
Upper ε	.0021
Lower ε	.01

where upper ε and lower ε stand for strain at the upper—i.e. most compressed—and lower—i.e. most tensed—side of the structure; y_n^p and y_n^e are the distances of the neutral axis from the bottom of the beam when complete plastic strain occurs and at the elastic limit, respectively.

The theoretical value of the limit moment allows us to calculate the limit load, as

$$M_y = F_y d \Leftrightarrow F_y = \frac{M_y}{d} \tag{5}$$

By using the quantity reported in Figure 4, one obtains

$$\begin{aligned} d &= 0.73m - 0.26m = 0.47m \\ F_y &= \frac{13.9kNm}{0.47m} = 29.6kN \end{aligned} \tag{6}$$

A typical record of strain obtained during the experiments is reported in Table 3. The diagram consists of several waves that represent the strains along the optical fiber for the different span paths. Since the length of the portion of the fiber that is embedded into the beam is known *a priori*, it is possible to relate the abscissa to the relevant cross-section and height within the beam. Hence, the strain shown in figure 7 actually represents a two-dimensional map of the strain over the beam.

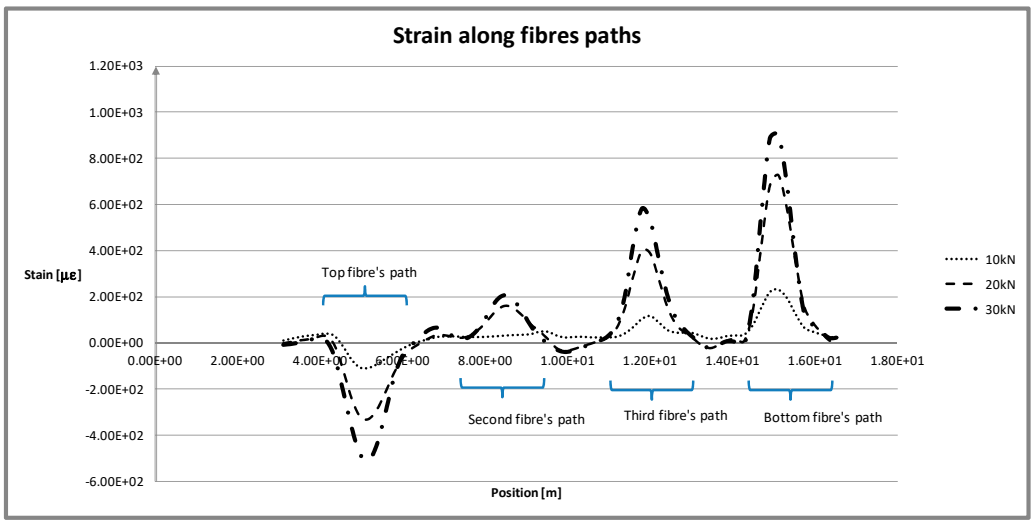

Figure 9: Strain recording along the fiber for different load steps

Preprints (www.preprints.org) | NOT PEER-REVIEWED | Posted: 18 July 2018 doi:10.20944/preprints201807.0331.v1

In the following Table 3, the strains at sections located at the mid-span of the beam, i.e. at a distance z from the left-wise support given by $z = 0.91m$ (see Figure 3), are reported; in the table, the beam curvature and bending moment, calculated analytically from recorded data, are reported as well. By assuming that the Bernoulli hypothesis on the plane cross-section holds, the curvature is calculated by

$$\chi = \frac{\varepsilon_l - \varepsilon_u}{h - c}, \tag{7}$$

where $h - c$ is the distance from the fibers along the cross-section height, $c = 20mm$ is the distance of the bars from the upper and the lower side of the section and h is its height.

Table 3. Results at mid span: z = 0.91 m.

Force [KN]	Lower ε	Upper ε	Curvature χ [1/m]	Moment [KN m]
0	0	0	0	0
10	0,000378	-0,0000516	0,002685	4,7
20	0,000837	-0,000082	0,00574375	9,4
30	0,00127	-0,000142	0,008825	14,1
40	0,00218	-0,000178	0,0147375	18,8
50	0,00476	-0,000225	0,03115625	23,5
40	0,00477	-0,000177	0,03091875	18,8
30	0,0058	-0,0000894	0,03680875	14,1
20	0,00733	0,0000021	0,04579938	9,4
10	0,00665	0,000226	0,04015	4,7
2	0,00641	0,000367	0,03776875	0,94

The theoretical limit response of the beam, as summarized in Table 2, allows us to notice that the conventional limit suggested by EC2 is lower than the measured limit; this confirms that the conventional limit prescribed by the normal accounts of safety factors is as it has to be expected and does not represent the actual behavior of the structure. The same comment holds with respect to the prescribed limit strain to be used in analytical calculation; more precisely, the standard resistant moment is assumed to correspond to the prescribed strain limits, which are reported in Table 2, even if these limits do not conform to the actual response of the structure.

The moment–curvature ($M - \chi$) diagram is drawn from recorded data; Table 3 reports the results concerning the cross-section at the middle of the beam span during the loading and unloading phases of the last load step, and analogous results have been elaborated in order to obtain the $M - \chi$ diagram for various cross-sections. In particular, in the following Figure 11, three significant diagrams are reported corresponding to the point where the force has been applied, the mid-span point and a point outside the load application range. The diagrams related to $z=0.73m$ and $z=0.91m$ are almost equal, thus confirming that, within the beam portion between the two acting forces, the moment is actually constant; moreover, one can see that the diagrams account for the snap back discontinuity of the moment, indicating that sudden cracks grow together with a non-linear occurrence. The diagram indicated by $z=1.26m$ refers to the point where the bending moment is less than the yield limit, although it is greater than the first crack growth limit. From the diagram, it can be seen that the curvature does not recover anymore at unloading, but no sudden decrease of the stress occurs, since it has to be expected that only micro-cracks develop at this stage. Finally, it can be seen, from any of three diagrams, that the linear part of the moment–curvature law is well recorded by the measurement device with a good agreement with theoretical expected values.

Preprints (www.preprints.org) | NOT PEER-REVIEWED | Posted: 18 July 2018 doi:10.20944/preprints201807.0331.v1

In order to check the measured strain during the non-linear response of RC beams, a comparison with the theoretical prediction has been reported hereafter.
For the scope, the actual neutral axis elevation with respect to the beam bottom line has been calculated by strain measures, both in elastic and plastic phases, y_n^e and y_n^p. In any case, the actual neutral axis elevation y_n depends on strain by means of the following linear equation:

$$y_n = c + \frac{\varepsilon_l}{\varepsilon_l - \varepsilon_u}\left(h - c\right) \tag{8}$$

Equation (8) has been used to obtain y_n during several load steps; in particular, the measurements have been permitted to calculate y_n during the last monotone load path. The results are summarized in the following table, and it can be seen that the neutral axis has moved upwards during crack propagation and non-linear strain occurrence.

Table 4. Neutral axis translation from elastic to plastic.

F	ε_l	ε_u	y_n
10	0.00038	-5.16E-05	0.160782
20	0.00084	-0.000082	0.165724
30	0.00127	-0.000142	0.163909
40	0.00218	-0.000178	0.167922
50	0.00476	-0.000225	0.172778

Such a behavior can be ascribed to the fact that the stress does not remain elastic anymore, and hence its result increases with respect to the linear case.
The beam is under elastic load for $F = 10kN$ and the neutral axis has the following elevation:

$$y_n^e = 0.02 + \frac{0.00038}{0.00038 + -5.16 \times 10^{-05}} 0.16 = 0.161m \tag{9}$$

The value of y_n^p in the plastic stage is calculated for $F = 50kN$ and is obtained by equation (8), hence

Preprints (www.preprints.org) | NOT PEER-REVIEWED | Posted: 18 July 2018 doi:10.20944/preprints201807.0331.v1

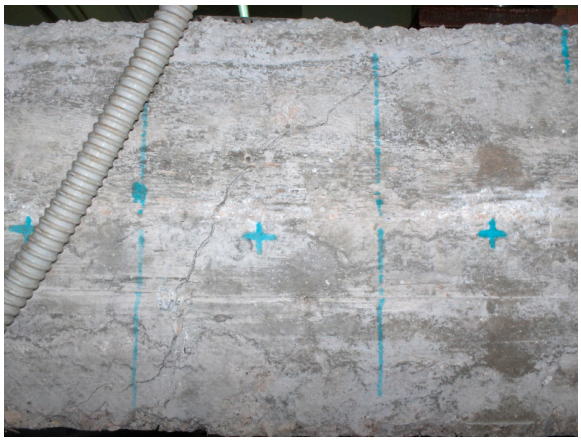

Figure 10: Cracks at the incoming collapse

$$y_n^p = 0.02 + \frac{0.00476}{0.00476 + 0.000225} 0.16 = 0.173m \tag{10}$$

This result can be compared with the theoretical one, equation (4), and that obtained by EC2 and reported in Table 2. The strain measurements obtained by means of the optical fiber sensor allow us to calculate the function of the curvature of the beam along its span; the curvature χ has been calculated by equation (7) and the bending moment by equation (5).

The picture in Figure 10 clearly shows that, at incoming collapse, the beam presents several cracks. The ruptures are of two types: the one at the lower edge of the structure consists of a crack that has to be imputed to the attainment of the tensile limit of the concrete; the other one, on the upper side of the beam, is due to the buckling of the compressed side outside the confined core of the beam by the brackets.

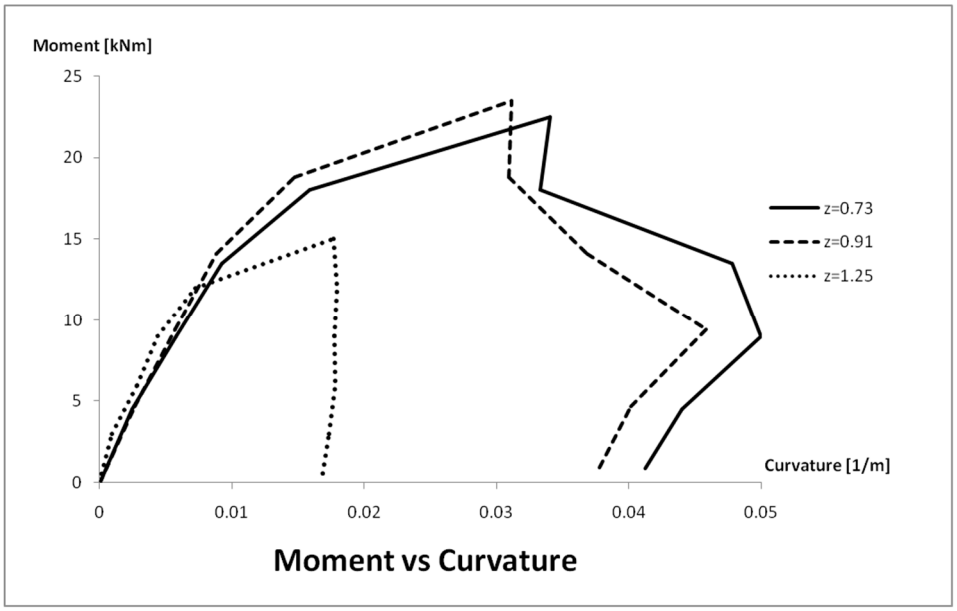

Figure 11. Moment–curvature diagrams for z=0.73, z=0.91, z=1.25 cross-sections.

The results confirm what is to be expected from the buckling analysis of the structure [31].

 doi:10.20944/preprints201807.0331.v1

5. Conclusions

The experiments reported have confirmed that Brillouin optical time domain analysis sensors can be used in civil engineering activities for structural monitoring. The experiments described in the present work concern laboratory structures instrumented with ordinary optical fibers for telecommunication. The fibers are very cheap and easy to set up as a sensor, and they make it possible to set up complicated sensor lattices with little effort in terms of time and resources.

A particular set-up has been tested: it is made of a single fiber that runs within the beam along four different paths at different heights. The fiber is embedded into the concrete during its casting and is supported by means of a light iron cable tensed between the steel brackets and the reinforcement bars.

The experimental setup has been designed to obtain results on the strain distribution within the structure in order to give information both on the feasibility of accurate internal measurement and on the actual strain distribution within concrete beams at non-linear—for instance, fracture and plasticity—stress levels. Moreover, the experiment confirms that the fiber did not break during installation, even if no particular attention has been paid to avoiding damaging the sensor; only an ordinary cure has been applied. Hence the sensor has shown its robustness with respect to damage at installation stage.

Moreover, it has been shown that the strain measurements obtained by means of BOTDA sensors can be used to get a continuous record along the structure and during the load time history with very good approximations. As a consequence of the experiments, it has to be stressed that concrete theoretical modeling has once more had its robustness confirmed, since the calculated limit for the bending moment and neutral axes positions are in good agreement with those obtained by experiments.

In conclusion, the proposed experimental setting that makes use of BOTDA has shown that the proposed sensors are suitable devices to monitor beam structural behavior continuously across space and time due to their reliability and to the low cost of the system, since it is very easy to apply long fibers within a concrete structure, or even to embed them into the concrete cast. The experimental results suggest that it is possible to design new configurations (i.e. to set several paths to be monitored in several different directions) such that it could be possible to obtain important information about the behavior of more complicated concrete structures. The BOTDA sensors can be used to monitor structures during their life and to confirm theoretical assumptions and calculations. This suggests the possibility of exploiting BOTDA from two different points of view: first, for scientific experimental investigation of structural response; second, for continuous monitoring of the health of existing infrastructures.

Author Contributions: The authors conceived and performed the experiments and elaborated the data in a substantially equal way.

References

1. G. W. Housner, L. A. Bergman, T. K. Caughey, A. G. Chassiakos, R. O. Claus, S. F. Masri, R. E. Skelton, T. T. Soong, B. F. Spencer and J. T. P. Yao. "Structural Control: Past, Present, and Future." *JoEM*, **1997.**
2. A. Katunin, K. Dragan and M. Dziendzikowski, "Damage identification in aircraft composite structures: A case study using various non-destructive testing techniques," *Composite Structures*, **2015.**
3. U. Polimeno and M. Meo, "Detecting barely visible impact damage detection on aircraft composites structures," *Composite Structures*, **2009.**
4. W. J. Staszewski, S. Mahzan and R. Traynor, "Health monitoring of aerospace composite structures - Active and passive approach," *Composites Science and Technology*, **2009.**
5. K. Diamanti and C. Soutis, "Structural health monitoring techniques for aircraft composite structures," *Progress in Aerospace Sciences*, **2010.**

6. B. Park, Y. K. An and H. Sohn, "Visualization of hidden delamination and debonding in composites through noncontact laser ultrasonic scanning," *Composites Science and Technology*, **2014.**
7. N. P. Avdelidis, D. P. Almond, A. Dobbinson, B. C. Hawtin, C. Ibarra-Castanedo and X. Maldague, "Aircraft composites assessment by means of transient thermal NDT," *Progress in Aerospace Sciences*, **2004.**
8. C. Meola and G. M. Carlomagno, "Impact damage in GFRP: New insights with infrared thermography," *Composites Part A: Applied Science and Manufacturing*, **2010.**
9. R. Usamentiaga, P. Venegas, J. Guerediaga, L. Vega and I. López, "Automatic detection of impact damage in carbon fiber composites using active thermography," *Infrared Physics & Technology*, **2013.**
10. I. Trendafilova, M. Cartmell and W. Ostachowicz, "Vibration-based damage detection in an aircraft wing scaled model using principal component analysis and pattern recognition," *Journal of Sound and Vibration*, **2007.**
11. D. D. Rizos, S. D. Fassois, Z. P. Marioli-Riga and A. N. Karanika, "Vibration-based skin damage statistical detection and restoration assessment in a stiffened aircraft panel," *Mechanical Systems and Signal Processing*, **2008.**
12. C. Ratcliffe, D. Heider, R. Crane, C. Krauthauser, M. K. Yoon and J. W. Gillespie, "Investigation into the use of low cost MEMS accelerometers for vibration based damage detection," *Composite Structures*, **2008.**
13. T. H. Loutas, A. Panopoulou, D. Roulias and V. Kostopoulos, "Intelligent health monitoring of aerospace composite structures based on dynamic strain measurements," *Expert Systems with Applications*, **2012.**
14 Y. Zou, L. Tong and G. P. Steven, "Vibration-based model-dependent damage (delamination) identification and health monitoring for composite structures - a review," *Journal of Sound and Vibration*, **2000.**
15. A. Katunin, "Vibration-based spatial damage identification in honeycomb-core sandwich composite structures using wavelet analysis," *Composite Structures*, **2014.**
16. C.-Y. Hong, J.-H. Yin and Y.-F. Zhang, "Deformation monitoring of long GFRP bar soil nails using distributed optical fiber sensing technology," *Smart Materials and Structures*, **2016.**
17. X. Huang, M. Yang, L. Feng, H. Gu, H. Su, X. Cui and W. Cao, "Crack detection study for hydraulic concrete using PPP-BOTDA," *Smart Structures and Systems*, **2017.**
18. M. Fajkus, J. Nedoma, P. Mec, E. Hrubesova, R. Martinek and V. Vasinek, "Analysis of the highway tunnels monitoring using an optical fiber implemented into primary lining," *Journal of Electrical Engineering*, **2017.**
19. Y. Stern, Y. London, E. Preter, Y. Antman, H. Diamandi, M. Silbiger, G. Adler, E. Levenberg, D. Shalev and A. Zadok, "Brillouin optical correlation domain analysis in composite material beams," *Sensors (Switzerland)*, **2017.**
20. H. Mohamad, A. B. H. Kueh and A. S. A. Rashid, "Distributed optical-fibre strain sensing in reinforced concrete structures," *Jurnal Teknologi*, **2015.**
21. X. Feng, J. Zhou, C. Sun, X. Zhang and F. Ansari, "Theoretical and Experimental Investigations into Crack Detection with BOTDR-Distributed Fiber Optic Sensors," *Journal of Engineering Mechanics*, **2013.**
22. X. Zhao, P. Gong, G. Qiao, J. Lu, X. Lv and J. Ou, "Brillouin corrosion expansion sensors for steel reinforced concrete structures using a fiber optic coil winding method," *Sensors*, **2011.**

23. Z. S. Wu, B. Xu, T. Takahashi and T. Harada, "Performance of a BOTDR optical fibre sensing technique for crack detection in concrete structures," *Structure and Infrastructure Engineering*, **2008.**

24. A. Barrias, J. R. Casas and S. Villalba, "A Review of Distributed Optical Fiber Sensors for Civil Engineering Applications," *Sensors*, **2016.**

25. X. Bao and L. Chen, "Recent progress in Brillouin scattering based fiber sensors," *Sensors*, **2011.**

26. J. E. Woods, D. T. Lau, X. Bao and W. Li, "Measuring strain fields in FRP strengthened RC shear walls using a distributed fiber optic sensor," *Engineering Structures*, **2017.**

27. P. Banerji, S. Chikermane, K. Grattan, S. Tong, F. Surre and R. Scott, "Application of fiber-optic strain sensors for monitoring of a pre-stressed concrete box girder bridge," *2011 IEEE SENSORS Proceedings*, **2011.**

28. K. Bremer, F. Weigand, Y. Zheng, L. Alwis, R. Helbig and B. Roth, "Structural Health Monitoring Using Textile Reinforcement Structures with Integrated Optical Fiber Sensors," *Sensors*, **2017.**

29. G. Rodríguez, J. Casas and S. Villalba, "Cracking assessment in concrete structures by distributed optical fiber," *Smart materials and structures*, **2015.**

30. Y. Wang, B. Jin, Y. Wang, D. Wang, X. Liu and Q. Dong, "Distributed fiber-optic vibration detection system," in 2016 13th International Conference on Ubiquitous Robots and Ambient Intelligence, *URAI 2016*, **2016.**

31. E. Ruocco and V. Minutolo, "Buckling Analysis of Mindlin Plates Under the Green–Lagrange Strain Hypothesis," *International Journal of Structural Stability and Dynamics*, **2015.**

32. G. Uva, F. Porco, A. Fiore and G. Porco, "Structural monitoring using fiber optic sensors of a pre-stressed concrete viaduct during construction phases," *Case Studies in Nondestructive Testing and Evaluation*, **2014.**

33. B. Glisic, D. Hubbell, D. H. Sigurdardottir and Y. Yao, "Damage detection and characterization using long-gauge and distributed fiber optic sensors," *Optical Engineering*, **2013.**